Geophysical Journal International

Geophys. J. Int. (2013) doi: 10.1093/gji/ggt163

Geophysical Journal International Advance Access published May 17, 2013

High-resolution relocation and mechanism of aftershocks of the 2007 Tocopilla (Chile) earthquake

A. Fuenzalida,[1] B. Schurr,[2] M. Lancieri,[3] M. Sobiesiak[4] and R. Madariaga[1]

[1] *Laboratoire de Géologie CNRS-Ecole Normale Supérieure,* 75231 *Paris Cedex* 05*, France. E-mail: fuenzalida@geologie.ens.fr*
[2] *GFZ German Research Centre for the Geosciences, D-*14473 *Potsdam, Germany*
[3] *Institut de Radioprotection et Sûreté Nucléaire,* 92262 *Fontenay-aux-Roses, France*
[4] *Geophysiks, Universität Kiel, Otto-Hahn-Platz* 1*,* 24118 *Kiel, Germany*

Accepted 2013 April 18. Received 2013 April 18; in original form 2012 August 6

SUMMARY

We study the distribution of the aftershocks of Tocopilla M_w 7.7 earthquake of 2007 November 14 in northern Chile in detail. This earthquake broke the lower part of the seismogenic zone at the southern end of the Northern Chile gap, a region that had its last megathrust earthquake in 1877. The aftershocks of Tocopilla occurred in several steps: the first day they were located along the coast inside the co-seismic rupture zone. After the second day they extended ocean-wards near the Mejillones peninsula. Finally in December they concentrated in the South near the future rupture zone of the Michilla intermediate depth earthquake of 2007 December 16. The aftershock sequence was recorded by the permanent IPOC (Integrated Plate Boundary Observatory in Chile) network and the temporary task force network installed 2 weeks after the main event. A total of 1238 events were identified and the seismic arrival times were directly read from seismograms. Initially we located these events using a single event procedure and then we relocated them using the double-difference method and a cross-correlation technique to measure time differences for clusters of aftershocks. We tested a 1-D velocity model and a 2-D one that takes into account the presence of the subducted Nazca Plate. Relocation significantly reduced the width of the aftershock distribution: in the inland area, the plate interface imaged by the aftershocks is thinner than 2 km. The two velocity models give similar results for earthquakes under the coast and a larger difference for events closer to the trench. The surface imaged by the aftershocks had a length of 160 km. It extends from 30 to 50 km depth in the northern part of the rupture zone; and between 5 and 55 km depth near the Mejillones peninsula. We observed a change in the dip angle of the subduction interface from 18° to 24° at a depth of 30 km. We propose that this change in dip is closely associated with the upper limit of the rupture zone of the main event. We also studied the focal mechanisms of the aftershocks, most of them were thrust events like the mainshock. As the aftershock activity was significantly reduced, on 2007 December 13, an M_L 6.1 event occurred offshore of the Mejillones peninsula reactivating the seismicity. Three days later the Michilla intraslab earthquake of M_w 6.8 ruptured an almost vertical fault with slab-push mechanism. The aftershocks locations of this event define a planar zone about 11 km in depth, situated right bellow the subduction interface.

Key words: Earthquake source observations; Subduction zone processes; South America.

1 INTRODUCTION

Northern Chile seismicity is dominated by the subduction of the Nazca Plate beneath South America. Subduction in Chile generates a large number of destructive earthquakes and tsunamis, like the recent Maule (M_w 8.8) earthquake of 2010 February 27 (Vigny *et al.* 2011) and the Valdivia megathrust earthquake of 1960 May 23 of magnitude M_w 9.5 (Kanamori & Cipar 1974; Cifuentes 1989). In an attempt to understand the occurrence of large earthquakes in the Chilean subduction zone several seismic gaps were identified in the 1970s and 1980s by Lomnitz (1971), Kelleher *et al.* (1973) and Compte *et al.* (1986). Gaps were defined as region that has not had a large earthquake in a long time, generally more than 50 yr for Chile. The geographical distribution and the extension of those gaps were based on historical descriptions mainly based on the work by Montessus de Balore (1911–1916) and are therefore affected by large uncertainties. The availability of new seismic and geodetic data has recently helped to identify more precisely the seismic gaps and their boundaries (Ruegg *et al.* 2009; Madariaga *et al.* 2010).

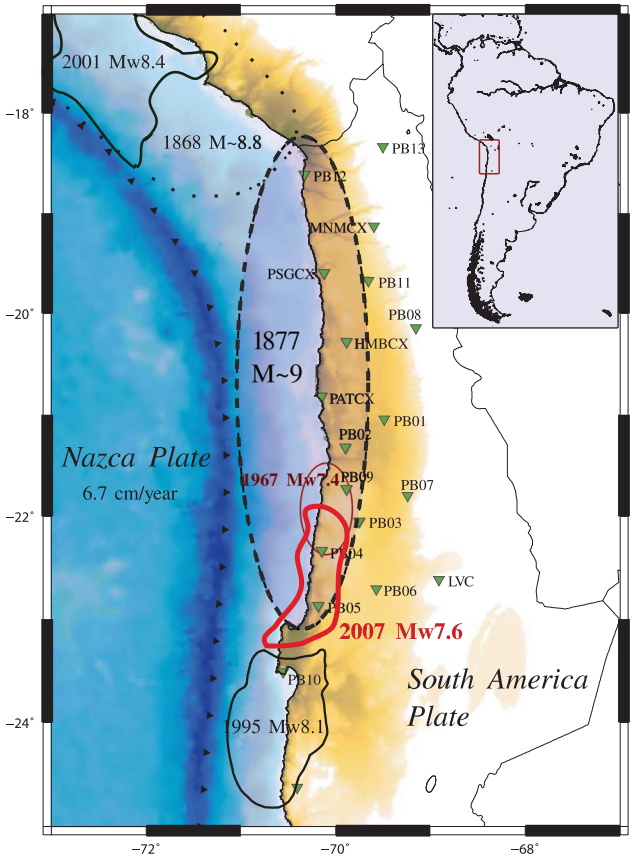

Figure 1. The Northern Chile seismic gap and the Tocopilla earthquake of 2007. The Northern Chile gap is the region that was broken by the $M \simeq 9$ Iquique earthquake of 1877. We show the rupture zones of the largest earthquakes of last century in the same area. The Tocopilla earthquake occurred in the Southern part of the gap. The permanent seismic stations of the IPOC network are shown with the green inverted triangles.

As shown in Fig. 1, one of the most conspicuous gaps in Chile is the Northern Chile Gap, that extends for more than 500 km from the city of Arica in the north to the Mejillones peninsula in the south, see for example Nishenko (1985). The last megathrust earthquake in this gap dates back to 1877, an event whose magnitude has been variously estimated between M_w 8.5 and 9 (Lomnitz 1971; Kausel 1986; Comte *et al.* 1986; Dorbath *et al.* 1990; Comte & Pardo 1991). The high rate of convergence of the Nazca Plate beneath the South American Plate (6.7 cm yr^{-1} according to Angermann *et al.* 1999) and the lack of large earthquakes in the last 135 yr make this area a very likely site for a future large earthquake. Currently the gap is surveyed by the permanent Integrated Plate Boundary Observatory (IPOC) network of Northern Chile (www.ipoc-network.org) deployed by Chilean, German and French researchers.

In the last 20 yr, two important earthquakes occurred just outside the boundary of the Northern Chile seismic gap: the 2001 June 23, M_w 8.4 Arequipa earthquake to the north and the 1995 July 30, M_w 8.1 Antofagasta earthquake in the south. The 2001 Arequipa earthquake broke the northern boundary of the gap and the contiguous area, covering part of the rupture zone of the 1868 event (Giovanni *et al.* 2002; Chlieh *et al.* 2011). The Antofagasta 1995 earthquake ruptured the region between 24.5°S and the Mejillones peninsula at 22.5°S (Ruegg *et al.* 1996; Delouis *et al.* 1997). The aftershock distribution (Delouis *et al.* 1997; Husen *et al.* 1999; Nippress & Rietbrock 2007) as well as the geodetic observations of this earthquake (Klotz *et al.* 1999; Pritchard *et al.* 2002; Chlieh *et al.* 2004) show that the Mejillones peninsula stopped the rupture transferring stresses into the southern part of the 1877 gap. In 2007, the Tocopilla earthquake of magnitude M_w 7.7 broke approximately 20 per cent of the Northern Chile gap releasing only a small amount of the accumulated stresses (Delouis *et al.* 2009; Béjar-Pizarro *et al.* 2010; Motagh *et al.* 2010; Peyrat *et al.* 2010). As shown in Fig. 1, in the area situated immediately in the North of Tocopilla an M_w 7.4 event occurred on 1967 December 21, studied by Malgrange & Madariaga (1983).

In the present paper, we study the aftershocks that followed the 2007 Tocopilla earthquake using 34 d of continuous recordings acquired by the IPOC network and by the German task force (TF) for earthquakes deployed 15 d after the mainshock (Sobiesiak *et al.* 2008) in the vicinity of the Mejillones peninsula. Because of the excellent quality of the available data we were able to perform a comprehensive analysis including event identification, accurate location, magnitude estimation and the determination of focal mechanisms. Our aim is to determine the aftershock area activated by the Tocopilla earthquake in order to study the following questions: what were the up and down dip limits of the rupture? Can these seismic observations define the subducted plate geometry? Did the Tocopilla earthquake activate upper-plate structures? And which are the focal mechanisms that played the main role in the broken area?

2 THE TOCOPILLA EARTHQUAKE

On 2007 November 14 the Tocopilla earthquake of magnitude M_w 7.7 (Delouis *et al.* 2009; Peyrat *et al.* 2010) broke the southern part of the Northern Chile gap. The slip distribution of this earthquake, shown in Fig. 2, was obtained by kinematic inversion of the source (Peyrat *et al.* 2010) using far and near field data. The slip distribution was composed of two main patches: the rupture started in the northern patch and propagated towards the south breaking a second patch that covers an area close to the ocean and stopped at the Mejillones peninsula. The results of seismic inversion were confirmed by interferometric synthetic aperture radar (InSAR) and global positioning system (GPS) observations (Béjar-Pizarro *et al.* 2010; Motagh *et al.* 2010; Schurr *et al.* 2012). The joint inversion of these geodetic data shows that the Tocopilla earthquake broke the subduction interface between 30 and 50 km depth. This observation is in agreement with the aftershock distribution of the first 24 hr following the Tocopilla earthquake (Delouis *et al.* 2009; Motagh *et al.* 2010; Schurr *et al.* 2012).

Two important aftershocks of M_w 6.8 and M_w 6.3 occurred on 15 November 2007, almost 24 hr after the mainshock, off-shore the Mejillones peninsula (Peyrat *et al.* 2010; Schurr *et al.* 2012). Both are thrust events with the same mechanism as the Tocopilla earthquake. In the same zone we identified five events of magnitude M_w larger than 6 that occurred during the first week after the Tocopilla earthquake (Lancieri *et al.* 2012; Schurr *et al.* 2012) (see Fig. 2).

Seismic activity after November 15 occurred mainly offshore to the north of the Mejillones peninsula until a strong intraslab event of M_w 6.8 occurred at the bottom of the seismogenic interface on 2007 December 16. This event, the Michilla earthquake, was situated inside the Nazca Plate at 46 km of depth, 5 km below the subduction interface. The Michilla earthquake and its main aftershocks had a slab-push mechanism characterized by an along the slab compression. This event had an almost vertical main rupture plane (Peyrat *et al.* 2010; Ruiz & Madariaga 2011). As discussed by Lemoine *et al.* (2002) and Gardi *et al.* (2006) this kind of earthquake has also been observed after other strong thrust events in Chile, Peru and Mexico and their origin is still a matter of debate.

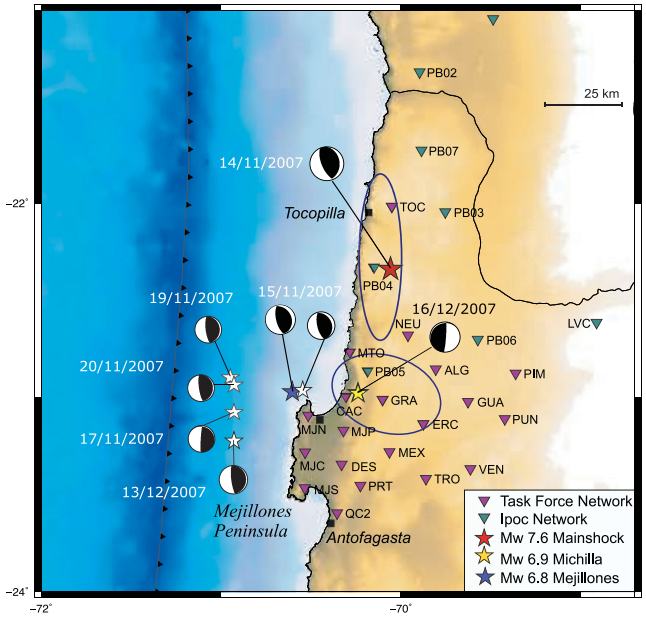

Figure 2. The M_w 7.7 Tocopilla earthquake of 2007 November 14. The epicentre of the main event is shown with a red star and the black ellipses show the slip patches of the main event determined by Peyrat *et al.* (2010). The focal mechanisms from the global centroid moment tensor catalogue show the main aftershocks of the event. Two shallow thrust aftershocks occurred on 2007 November 15 offshore Mejillones peninsula. The slab-push event of M_w 6.9 of 2007 December 16 is shown with a yellow star. The stations of the task force (TF) seismic network that was deployed 2 weeks after the mainshock are shown with magenta triangles. The green triangles depict the location of the permanent IPOC network.

3 SEISMOLOGICAL DATA

The Tocopilla aftershocks were locally recorded by the IPOC and TF networks in the North of Chile (Fig. 2). The IPOC network was installed in 2006 thanks to an agreement between the International Laboratory Montessus de Ballore (LIA) and the German Research Centre for Geosciences (GFZ) with the aim of monitoring the seismic gap of northern Chile. The IPOC network was composed of 12 stations equipped with broadband seismometers (STS-2) and accelerometers (GMG-5 and Episensor FBA ES-T), spanning the northern Chile gap with an inter-station distance of 80 km. The network was operational in 2007 November when the main event and the entire aftershock sequence were recorded at the seven southernmost stations (Fig. 2). The PB04 station was located right above the hypocentre of the main event and station PB05 was situated above the Michilla slab-push event of 2007 December 16. The IPOC network has been continuously improved and is currently operational in Northern Chile. In order to understand the activity of the southern part of the rupture, from 2007 November 29 a temporary network TF was deployed around the Mejillones peninsula (Sobiesiak *et al.* 2008). The network was composed of 20 mostly short period instruments (L4-3D) recording continuously with a sampling rate of 100 Hz; the average distance between these stations was 15 km.

4 AFTERSHOCK LOCATIONS

4.1 Event detection

Intense aftershock activity requires a sophisticated method for the identification of events because their records often overlap in the seismograms and the coda of the events raises the level of background noise. We chose to use the Filter Picker detection algorithm of Lomax *et al.* (2012), which is an extension of the Allen (1978) and Baer & Kradolfer (1987) methods. It is specifically designed to operate on continuous, real-time (but in this case we had off-line data), broadband signals so as to avoid excessive triggering during large events. We set the threshold parameters of Filter Picker so that it could detect as many of the events of M_w larger than 2 as possible.

The association procedure (binding) analyses the *P* wave arrival times at every station to determine whether they are compatible with propagation across the network from a common source (Lancieri *et al.* 2011). This technique is based on the coincidence of a minimum of five picks within a given time window. We then automatically cut windows of 3 min (60 s before and 120 s after the *P* phase) around each of the events that were identified. During the first 2 weeks, when only the IPOC network was available, we were not able to locate all the detected events; this is due to the high seismic activity and the large distance between the stations, the recorded *P* phase were often hidden by the *S* phase or the coda of the previous events. After the TF installation the distance between stations was reduced, improving the detection capacity. Thanks to the stations located on the Mejillones peninsula the offshore events were also better located.

In order to obtain the best possible locations, we manually determined the arrival time of *P* and *S* phases on the seismic traces using the seismic analysis code (SAC) of Goldstein *et al.* (2003). We also read the *P*-phase polarities to determine focal mechanisms. Overall we located 1238 events, 500 from November 14 to 28 when only the IPOC network was available, and 738 from November 29 to December 17 after the deployment of the TF network (see Table 1).

4.2 NonLinLoc locations

The precision of the hypocentre location depends on the quality and number of phase readings, the spatial distribution of the stations and a good knowledge of the velocity model. The good waveform data of Northern Chile along with the manual reading of arrival times permitted us to build an accurate catalogue of events. The events were first located with the NonLinLoc software (Lomax *et al.* 2000) using two different velocity models (Fig. S1). We tested (1) a 1-D velocity model derived by Husen *et al.* (2000) from the study of the aftershock sequence of the 1995 Antofagasta earthquake, where onshore and offshore instruments were available. And (2) a 2-D velocity model inverted by Patzwahl *et al.* (1999) from the records obtained during the CINCA seismic refraction project located just north to the Mejillones peninsula.

The 1238 events located with the 1-D and 2-D velocity model are shown in Figs 3(a) and (b), respectively. The epicentres derived with either of the two velocity models are quite similar. The aftershocks were mostly located on the two slip patches of the main event plus a significant amount of aftershocks situated offshore of the Mejillones peninsula (Figs 3a and b). The depths of the events located using these two models were quite different for the events located closer to the trench, as can be observed in the vertical cross-sections plotted in Figs 3(c)–(f). The aftershocks of the Michilla earthquake of 2007 December 16 were located very close to an almost vertical plane inside the Nazca Plate; results are the same when using either one of the two structural models.

As shown in Table 1, we divided the catalogue into three periods of time according to differences in coverage and seismic activity:

Table 1. Summary of depth errors for the two velocity models used to locate the aftershocks.

Period	Network	Date	Located events	Magnitude	M_w range	Error 1-D (km)	Error 2-D (km)
I	IPOC	2007 November 14–2007 November 28	500	M_w	[2.6–7.8]	–	–
II	IPOC + TF	2007 November 29-2007 December 15	487	M_L	[2.2–6.2]	1.73	2.15
III	IPOC + TF	2007 December 16–2007 December 17	251	M_L	[1.8–6.8]	0.78	1,20

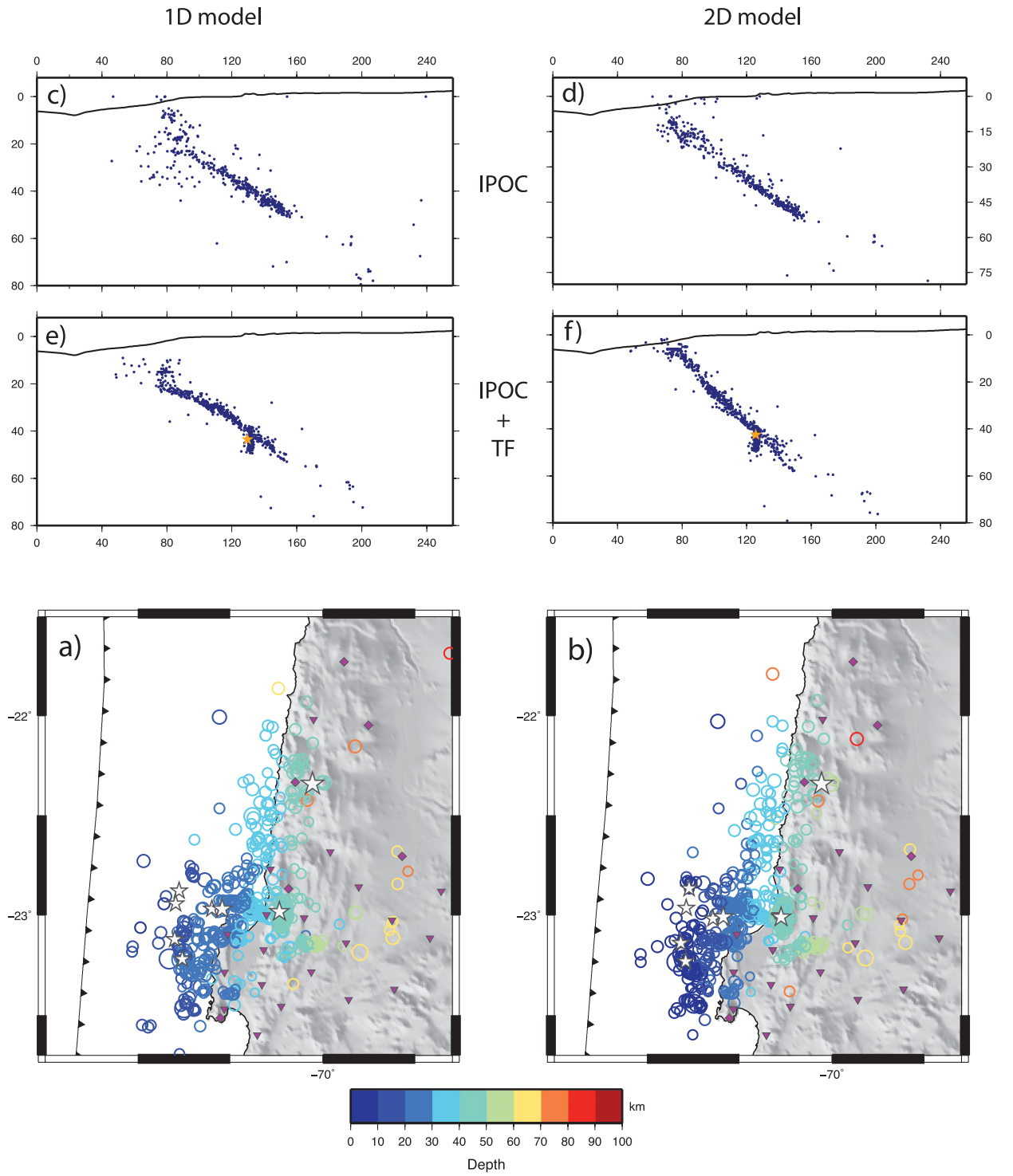

Figure 3. Hypocentral locations of the aftershocks of the Tocopilla earthquake of 2007 November 14 obtained with the Nonlinloc software. On the left-hand side, we plot the locations obtained with the 1-D velocity model proposed by Husen *et al.* (2000). On the right-hand side, the locations determined using the 2-D model proposed by Patzwahl *et al.* (1999). Above the plan views we show E–W cross-sections of the aftershocks. On (c) and (d), we plot the hypocentres determined in period I when only the IPOC network was available. (d) and (f) are the locations obtained when both the Task Force and IPOC network were operational.

Period I covers the first 2 weeks of aftershocks of the Tocopilla earthquake (cross-section on Figs 3c and d), when only seven IPOC network stations were available; period II extends from the TF installation until the occurrence of the Michilla earthquake on December 16 (20 additional stations); period III includes the Michilla earthquake and 2 d of its aftershocks. The events that occurred during periods II and III were located using both the TF and IPOC networks and are shown by the cross-sections of Figs 3(e) and (f).

The solutions obtained for the first period using each of the two velocity models provide a clear image of the subduction interface. The events located offshore and in the southern area show a certain dispersion due to poor azimuthal coverage by the IPOC network. The 2-D model produced locations that were less scattered compared to those obtained with the 1-D model but both have large errors in depth. For periods II and III, after the installation of the temporary TF network, the dispersion of hypocentre distribution was significantly reduced (Figs 3e and f). The hypocentres obtained from the 1-D model (Fig. 3e) are distributed along a thin surface with a dip angle that decreases as the events get closer to the trench. The distribution of aftershocks located using the 2-D model images a subduction interface that has a constant slope, so that the offshore events reach the surface about 10 km from the trench.

To determine which velocity model provides the best locations, we looked at the uncertainties of hypocentral depth. We focused on depth because this is the parameter affected by the largest errors. Table 1 summarizes the depth errors computed from the covariance matrix derived for the two velocity models (Lomax *et al.* 2000).

As expected, the errors increase towards the trench for the two models (Fig. S2). During period I, the network geometry dominated the uncertainties, so that we were not able to decide which model produced better locations based on the formal errors. For period II (see Table 1), the errors in depth determination were improved with a mean value of 1.73 km for the 1-D model and 2.15 km for the 2-D model. Finally for period III, the errors were smaller because the Michilla earthquake and its aftershocks were located inland, just below the TF network. We obtained a mean error of 0.78 km for the 1-D and 1.20 km for the 2-D models. In conclusion, the 1-D model produce locations with smaller errors than the 2-D model, but the difference between them may not be very significant. The influence of the velocity model particularly on the depths of the off-shore events is significant and has to be kept in mind for the interpretations.

4.3 Double-difference relocation

In order to improve the location of clusters of repeating aftershocks, we used the double-difference (DD) relocation algorithm (Waldhauser & Ellsworth 2000). The DD method relates traveltime differences of pairs of nearby events recorded by the same instrument to their spatial separations and therefore cancels out the correlated errors arising from unmodelled structure along the segment of the path that they share. The DD method has been shown to be particularly effective if precise differential traveltimes are measured using waveform cross correlation. Cross correlation-based traveltime differences are often an order of magnitude more precise than those derived from manually picked earthquake catalogues. We focus our relocation analysis on periods II and III of the data set starting from 2007 November 29; these include the dense TF station network. Cross correlations for *P*-phases were computed from the vertical components after applying a 3-pole causal 1–10 Hz Butterworth bandpass filter for windows from 0.5 s before to 1.5 s after the *P*-wave pick. For *S* phases horizontal components were windowed from 1.0 s before to 2.0 s after the *S*-wave pick. For *S* phases the same frequency filter as for *P* phases was used and in addition traces were integrated to displacement because we found that this enhanced the *S* signal. For the *S* phase windows, we stacked the cross-correlation function of the two horizontal components and obtained the lag time and correlation coefficient from the maximum amplitude of the stack. Lag times with a correlation coefficient >0.7 were saved for the relocation, using the correlation coefficient as a weight for the hypocentre inversion. We calculated the cross-correlation function for event pairs with a maximum epicentral separation of 15 km. This procedure yielded 27 117 cross correlation *P* lag time measurements and 29 198 cross correlation *S* lag time measurements. The event separation threshold was incrementally reduced to 5 km during the relocation procedure. As velocity model we used the 1-D model of Husen *et al.* (1999).

Fig. 4 shows the location obtained after the DD relocation. The northern aftershocks were located on an elongated zone that extends between 30 and 50 km depth (Fig. 4a). The aftershock zone is much larger in the southern part as shown in Figs 4(b) and (c), where the events were distributed between 5 and 55 km depth. In this area, a change in the dip angle of the aftershock distribution is clearly observed in the cross-section of Fig. 4(b). This change in dip angle from 18° to 24° occurs at a depth of 30 km under the coastline. The DD relocations reduce the width of the aftershock distribution to a thin layer about 2 km of thickness that we identify as the subduction interface. A comparison between locations before and after DD relocation is presented in Fig. S3 of the supplementary material. In Fig. 5 we show a zoom on the aftershock locations pointing out some interesting features.

5 CHARACTERIZATION OF SEISMICITY

5.1 Magnitude estimation

Once we built a catalog of aftershocks, we computed local magnitudes and focal mechanisms. For the first period of data, Period I in Table 1, a moment magnitude catalogue (M_w) was computed using the Brune (1970) spectral analysis of ground acceleration waveforms (Lancieri *et al.* 2011). That technique could not be applied to the second period because the TF network had only short period instruments. Many events of this second period were recorded at only two IPOC stations. For period II and III, when the largest number of stations was available, we evaluated the local magnitude using the Kanamori & Jennings (1978) procedure. This local magnitude (M_L) is defined as the logarithm of the maximum displacement measured by a Wood–Anderson torsion seismograph at an epicentral distance of 100 km (Richter 1935):

$$M_L = \log A + \log A_0 \quad (1)$$

where A is one half the peak-to-peak displacement A_{wa} weighted by distance R by the relation: $A = A_{wa} * R/100$. A_0 is the reference amplitude $\log A_0(R = 100\,\text{km}) = -3$.

For all the short-period seismograms the mean value and linear trend was removed before processing the data. The signals were deconvolved from instrumental response and re-convolved with the response of a Wood–Anderson instrument. We determined the maximum amplitude of the *S* wave on the horizontal components and corrected for the epicentral distance to evaluate the local magnitude

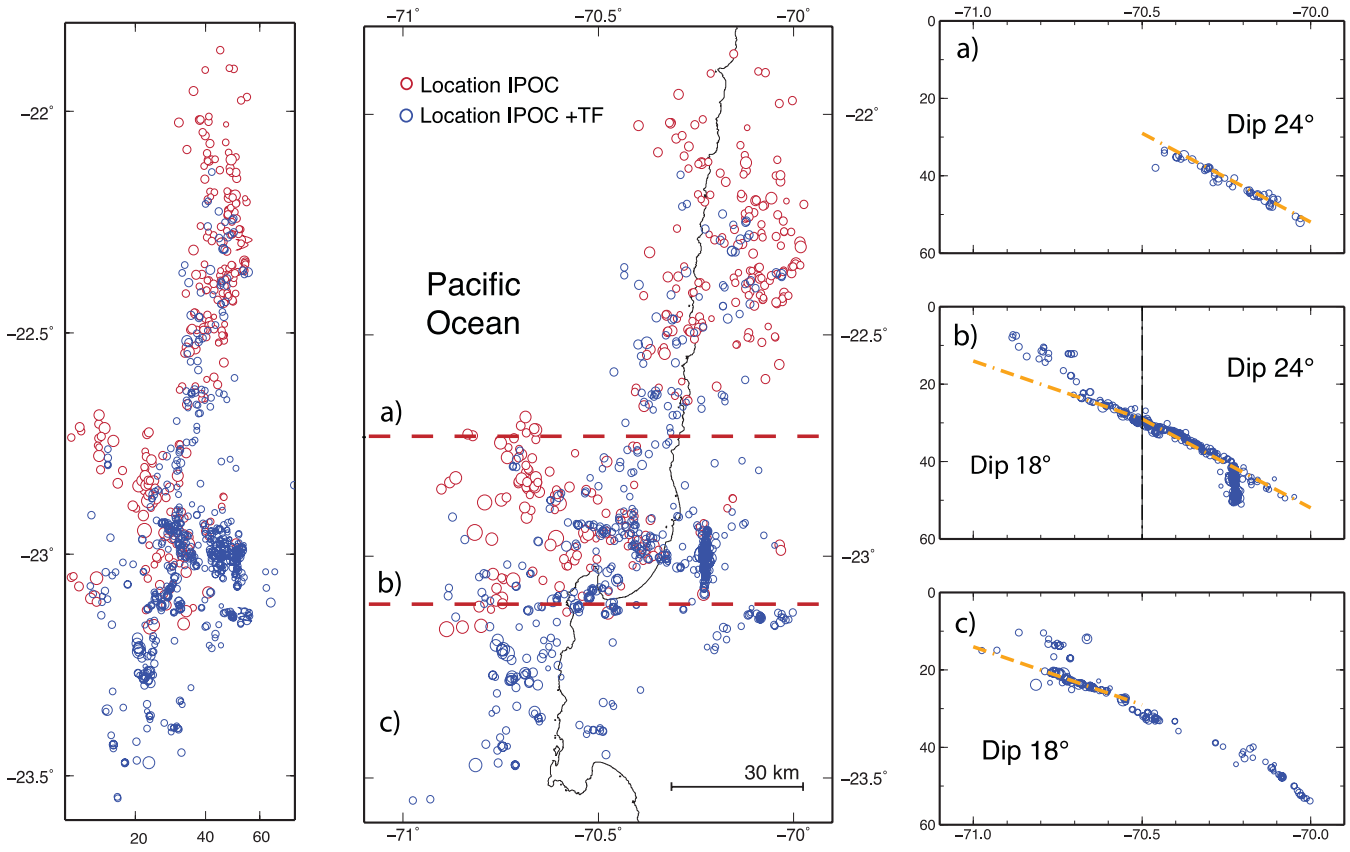

Figure 4. Joint double-difference relocations applied to event pairs with a maximum epicentral separation of 15 km and waveform cross-correlation coefficients >0.7. On the left-hand side, we show the N–S vertical cross-section of the relocated events for all the sequence. In the centre, we plot their geographical distribution, plotting with red the relocated events that occurred during the first 2 weeks and in blue those that took place after the TF installation. The E–W cross-sections (at the right-hand side) are plotted only for the second period because of their much better resolution. The aftershocks extend between 30 and 50 km depth in the northern area (a) and between 5 and 55 km (b and c) depth in the Mejillones peninsula zone. A dip change from 18° to 24° is observed under the coastline at a depth of 30 km.

at each station. Finally, for each event we took the average of all stations following the procedure proposed by Bobbio *et al.* (2009).

Fig. S4 of the supplementary material shows the number of events as a function of local magnitude interval for the three periods defined in Table 1. The first period had the broader range of magnitudes with several strong events : six events of magnitude larger than 6, and 33 larger than 5. Unfortunately, the geometry of the network did not permit us to locate smaller events, especially in the southern and offshore areas where the activity was the strongest. This situation improved with the installation of the TF network, but this period was less active with only one event with magnitude M_L larger than 6, and six events of M_L larger than 5. The third period corresponds mainly to the aftershocks of the Michilla earthquake. In this period, we had a very good azimuthal coverage necessary to locate a large number of events, including those events with smaller magnitudes. The b-value of the Gutenberg–Richter law was computed for the periods I, II and III. Its value was close to 1 for the ranges [3.6–6], [3–5] and [3–5], respectively (see Fig. S4).

With the goal of standardizing the two catalogues of magnitude obtained for the two different geometries, we had to study the lower magnitude thresholds. For magnitudes larger than 3 the effect of changing the network on aftershock location was very strong. On the other hand, if we choose a cut off magnitude of 4, the number of events that appear in both catalogues becomes very small. For this reason we made the space–time analysis in Section 6 using only local magnitudes M_L greater than 3.5.

5.2 Focal mechanisms

We determined the focal mechanism of the aftershocks from the first motions of *P* waves read directly from the seismograms that were used for the aftershock location in the previous sections. The FPFIT software (Reasenberg *et al.* 1985) was used to compute the focal mechanisms of the events having more than six polarity readings. We read the polarities from the vertical seismograms at each station and weighted it based on the signal to noise ratio. Using the incidence angles obtained from our locations, we determined the focal mechanisms for epicentral distances less than 110 km. This distance corresponds to the critical distance of the Pn phase arrival. For period I, the number of readings and the distance between stations was not enough to define robust fault plane solutions. For this reason we determined only the mechanisms of the events that occurred after the TF network installation. Mechanisms for period I were determined by Schurr *et al.* (2012) using moment tensors determined from wave form modelling at regional distances.

We obtained 231 mechanisms in period II, before the Michilla earthquake, with well resolved solutions, meaning errors of less than 30° in strike, dip and rake (Fig. 6). Most of them are thrust events just as the Tocopilla mainshock, and a significant part of them were located offshore. Unfortunately, in the offshore area the azimuthal coverage is less good so that the mechanisms are less well resolved. Inland, in the deeper seismogenic zone we observe a larger variability in the focal mechanism, including a few along-slab

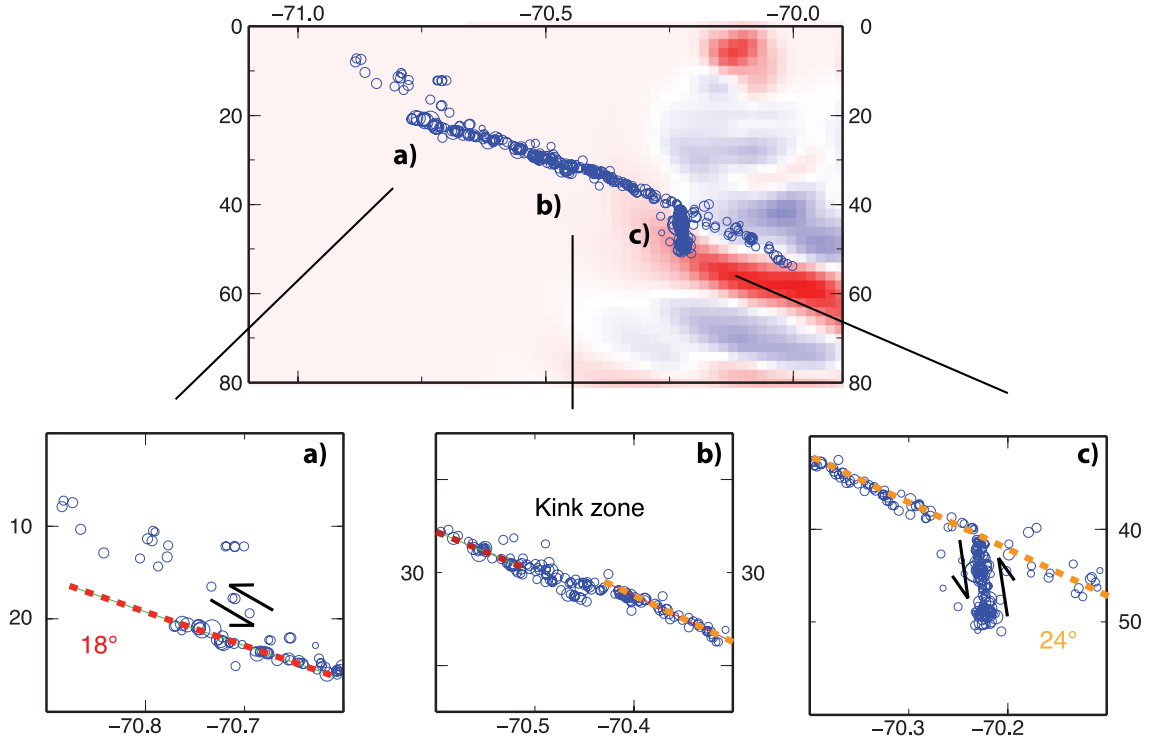

Figure 5. Detailed image of the cross-section under the Mejillones peninsula. In (a) relocated events show that some events split from the interface delineating a possible splay fault; in (b) at the depth of the kink we observe a small branch that penetrates into the Nazca Plate; and in (c) the aftershocks of Michilla earthquake broke the oceanic crust of the Nazca Plate along an almost vertical plane that penetrates 11 km into the subducted slab. In the background of the main cross-section in the top frame we plot the receiver function section computed by Sodoudi *et al.* (2011), migrated using the 1-D velocity model of Husen *et al.* (2000). The strong red phase is interpreted as the oceanic Moho, so that the Michilla earthquake seems to have broken the entire oceanic crust.

tensional mechanisms (slab-pull) such as the M_L 4.6 event of 2007 December 15 (Fig. 6). A short sequence of aftershocks started with the M_L 6.1 thrust event of 2007 December 13; this event triggered several M_L 5 events for which we could determine their mechanisms. The rose diagram in Fig. 7 summarizes the fault angles computed for events with dip errors less than 20°. We observe that most of the events had dips between 15° and 30°. We see no evidence of non thrust events in our catalogue as those found by Schurr *et al.* (2012) at shallow depths in the upper plate; those events occurred during he first week of aftershock when the TF was not yet in operation.

The focal mechanism of the Michilla earthquake (in red in Fig. 7) had an along the slab compression mechanism (slab-push). As shown in the figure this event occurred on an almost vertical plane inside the Nazca Plate at 46 km depth. Its aftershocks (plotted in red) and foreshocks (in blue) are shown in Fig. 8. The foreshocks occurred during the 2 weeks that preceded the Michilla event and had moderate magnitude ($M_L \simeq 3$) with a similar slab-push mechanism to Michilla event. In the rose diagram presented as an inset in Fig. 7 we observe that almost all the aftershoks had a rake angle close to 90°. We also found two preferred angles of dip: a steeper one close to 80° similar to that of the slab-push Michilla earthquake, and a second dip angle close to 25° that is typical of the thrust events of the main Tocopilla event. Thus inside the aftershock zone of the Michilla earthquake most events have the same mechanism as the slab-push event, but there are still a few shallow dip slip thrust events.They can be seen in Fig. S4.

6 SPACE–TIME DISTRIBUTION

The aftershock sequence of the Tocopilla earthquake is characterized by three main zones of activity: the area broken by the mainshock located inland; a strong activity off the Mejillones peninsula and the fore- and aftershock sequence of Michilla event. The temporal evolution of the events including their magnitude are shown separately for the two areas in Fig. 8: inland (plotted in red) and offshore (blue).

For the events located inland the activity started with the main Tocopilla event shown with a large star and its aftershocks were of moderate magnitude. Two patches of seismicity are highlighted: the events associated with the mainshock rupture area and the seismicity that was triggered offshore of the Mejillones peninsula producing two events of M_w 6.8 and another one of M_w 6.3 are indicated with the left-hand arrow. Seismicity remained high during the first week, with several events of magnitude greater than 6. It was reactivated several times and eventually became quieter during the second and third week of aftershocks. Finally, the offshore area was reactivated by the M_L 6.1 event that occurred on 2007 December 13. Some events migrated to the deeper parts of the seismogenic zone during the 3 d that preceded the Michilla earthquake of 2007 December 16.

7 DISCUSSION

The 2007, Tocopilla earthquake is one of the best instrumented earthquakes in Chile. Thanks to the IPOC network installed before the earthquake, we were able to study the principal features of the mainshock and its larger aftershocks (Peyrat *et al.* 2010; Schurr *et al.* 2012). Northern Chile offers ideal conditions for the study of seismicity because site effects are very limited and attenuation is low as discussed by Lancieri *et al.* (2012). In the 2 weeks that followed the main event, most of the aftershocks occurred offshore and in the southern part of the main rupture, where there were fewer

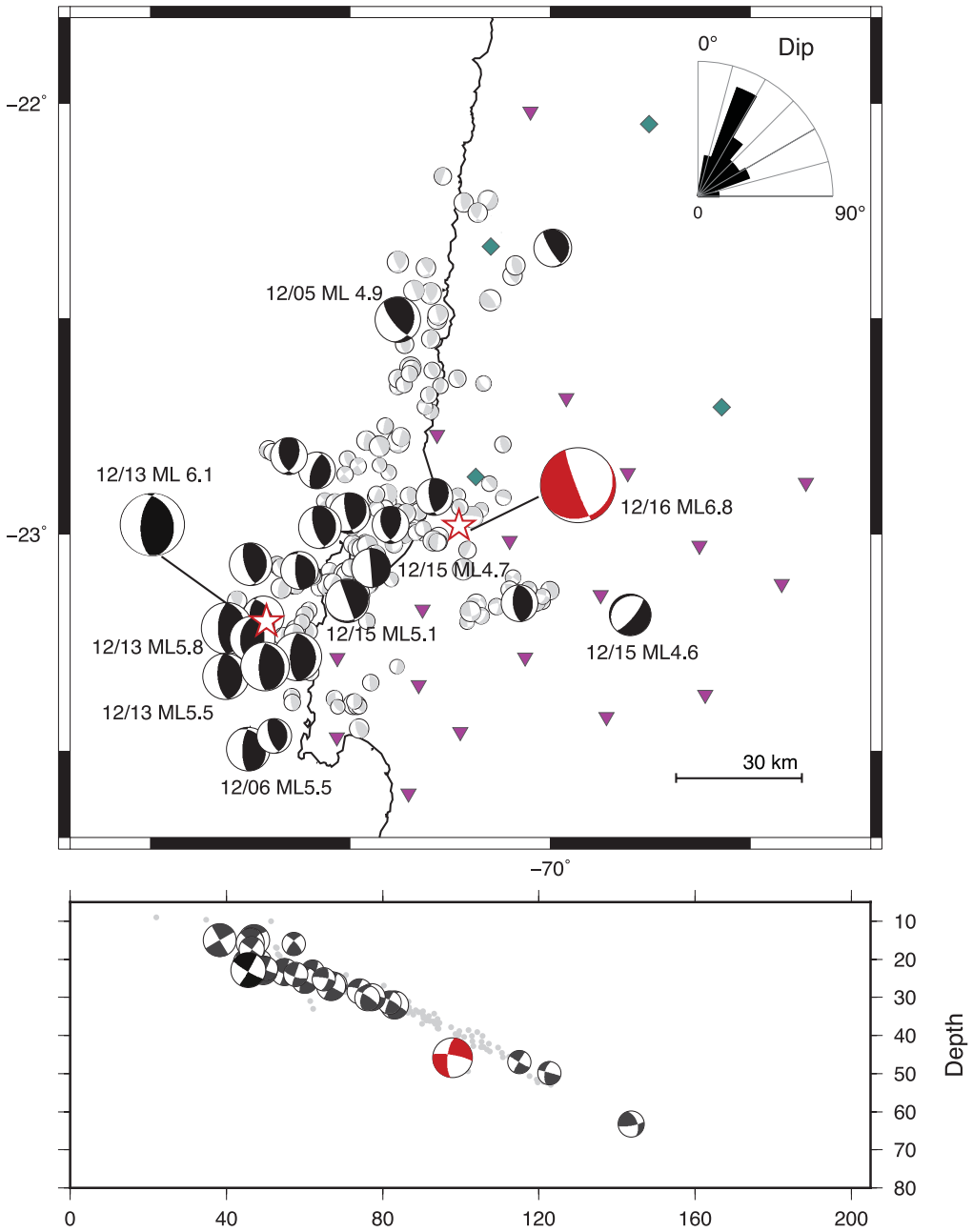

Figure 6. Focal mechanism of the aftershocks of the period from 2007 November 29 and 2007 December 16 when the TF network was recording. The rose diagram in the upper right-hand side shows the dip angles of the fault planes which are clearly dominated by an angle of 18°. The events of magnitude larger than 4.5 are highlighted in black and events of smaller magnitude are shown in grey. The Michilla (slab-push) and the M_L 6.1 event of 2007 December 13 epicentres are represented by stars.

stations installed before the earthquake. For this reason, we were not able to locate all the events that were identified by the automatic event picking algorithm. This situation improved significantly once the TF network was installed. The quantity of instruments and its spatial distribution allowed us to better identify seismic arrivals and reduce the error of locations particularly of southern and offshore events.

The location of the aftershocks situated offshore of the Mejillones peninsula was significantly affected by the velocity model used for the determination of hypocentres (see Fig. 9). We tested two velocity models that had been proposed for the region by earlier studies. A 1-D model determined for the aftershocks of the 1995 Antofagasta earthquake by Husen *et al.* (1999), and a 2-D model obtained by Patzwahl *et al.* (1999) for a seismic profile at the latitude of Tocopilla. The main difference in the locations is in the depth distribution of offshore events: the locations obtained using the 1-D model define a surface that smoothly joins the trench. Locations obtained with the 2-D model, on the other hand, define a plane that intersects the seafloor 10 km inland from the trench. We think that the 1-D velocity performs better for this zone because the errors were smaller, nevertheless it is less realistic because it lacks the slab. Locations obtained with the 1-D model define a dip angle of the plate interface that is in very good agreement with previous studies of the seismicity in the vicinity of Antofagasta, that imaged a plate interface zone with dip angles in the range from 17° to 18° (Comte *et al.* 1994; Delouis *et al.* 1996).

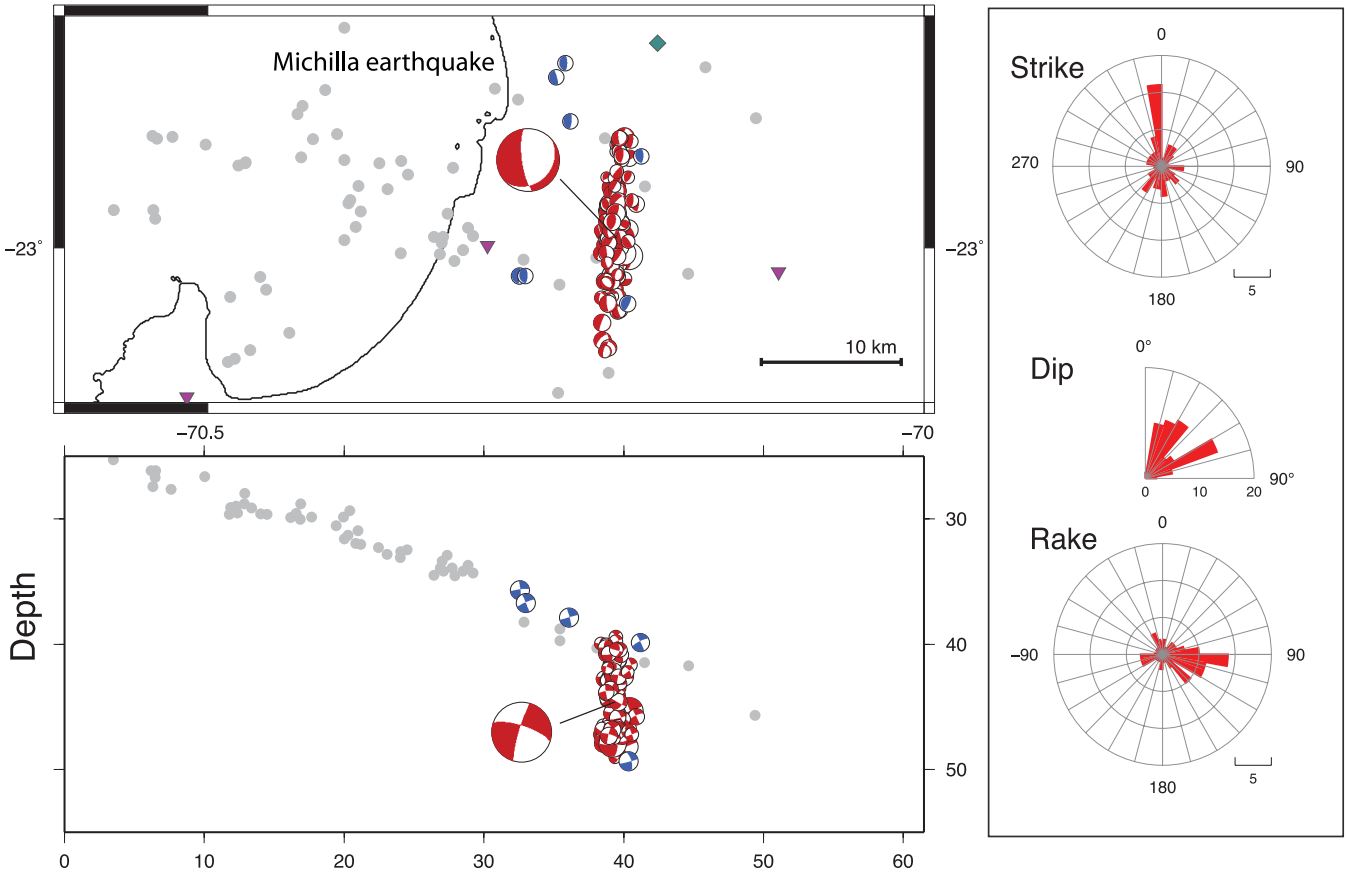

Figure 7. Focal mechanisms of the aftershocks of the Michilla earthquake of 2007 December 16 (in red) and seven of its foreshocks that occurred near its fault plane (in blue). Grey circles represents the background seismicity. Triangles and diamonds represents the nearby seismic stations.The rose diagram to the right-hand side of the figure shows that there were two dominant mechanisms during this period: thrust events with dip angles between 1° and 30° and slab compression events (slab push) with dip angles close to 60°.

Relocation using cross correlation of clusters of aftershocks significantly reduced the width of the seismogenic structures; aftershocks collapsed into a very thin surface of a thickness of about 2 km that we interpret as the shear zone located in the immediate vicinity of the plate interface. In Fig. 5, we zoom on the cross-section of Fig. 4(b). Three main features are evident: a shallow structure appears to detach from the subduction interface (Fig. 5 a) in the offshore zone; in the region of the kink, shown in Fig. 5(b), we observe that the hypocentres do not delineate a single layer but a small branch appears near −70.5°. Finally, as shown in Fig. 5(c), the Michilla earthquake rupture zone is clearly delimited by its aftershocks that define an 11 km depth section situated immediately below the subduction interface.

The kink found from the 1-D locations across the Mejillones peninsula increases the dip angle by about 6 degrees as observed in Fig. 5. Unlike the study of Contreras-Reyes *et al.* (2012), the change in dip angle of our aftershock distribution is situated at 30 km depth, instead of 18 km as proposed by them. Our locations do not image an abrupt change of dip but rather a broad zone of about 10 km width in the E–W direction (see Fig. 5 b). We observe the presence of a small seismicity branch inside the Nazca Plate right under the kink zone. The location of this change in dip corresponds to the upper limit of the aftershock distribution of the northern part of the Tocopilla earthquake. It is tempting to associate this kink with the arrest of the rupture, but other authors (Schurr *et al.* 2012) have suggested that the main event was stopped by a change in frictional properties of the plate interface. We have no data that is relevant to resolve these two hypotheses, although the change in frictional properties may be associated with the change in dip of the plate interface. To improve the geometry of the plate interface near the trench we would need ocean bottom instruments in order to resolve variations on the dip angle using the same localization methods.

In the inland zone, we did not find any evidence of activity at shallow depths, as could have been expected for some recent normal faults in the Mejillones peninsula plotted in Fig. 10 after (Armijo & Thiele 1990; Victor *et al.* 2011; Vargas *et al.* 2011). We observe a strong seismic activity under the Mejillones peninsula below these faults, but these events have depths of about 30 km, so that they are close to the plate interface. The only evidence of shallow seismicity is in the offshore area of the Mejillones peninsula: a cluster of aftershocks located in the upper plate that may be due to a possible splay fault (see Fig. 5 a). As we have already discussed those events are not sufficiently well located because of the lack of ocean bottom instruments. Another interesting observation is the diagonal alignment of seismicity just north of Mejillones peninsula in the offshore area. This alignment is not related to known geological structures and could be interpreted as due the presence of fluids as was proposed by Nippress & Rietbrock (2007) for the aftershocks of the Antofagasta earthquake, but this hypothesis needs to be confirmed by other observations.

The focal mechanism of almost all well located events was thrust faulting, typical of subduction events. A significant part of these events was located offshore where fault plane solutions are not well constrained due to poor azimuthal coverage. For period I,

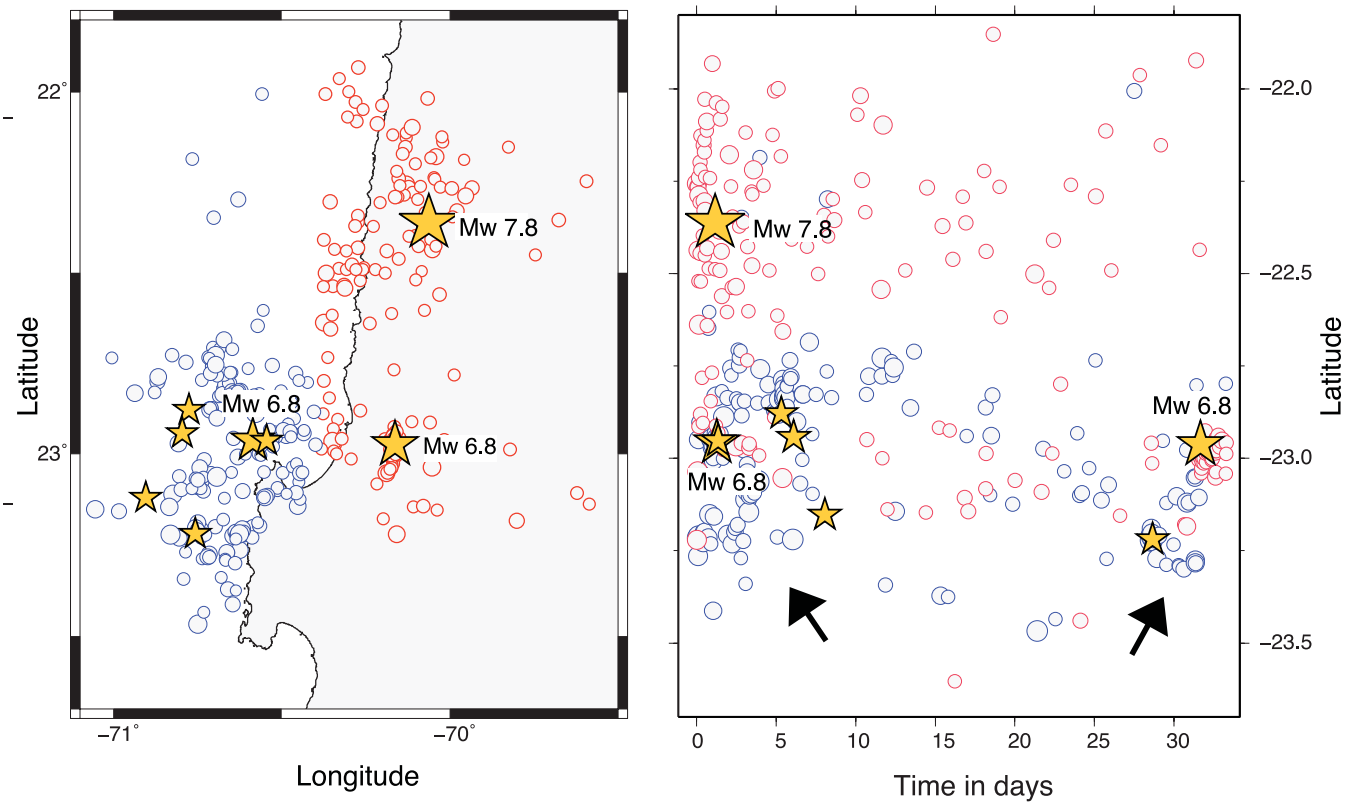

Figure 8. Migration of seismicity during the Tocopilla aftershocks of 2007. The catalogue is separated into inland (red) and offshore (blue) zones. On the right-hand side, we plot the space–time evolution of seismicity, the ordinate represents the latitude and the abscissa the time in days. The figure shows the patches of seismicity for the mainshock (the large yellow star in right-hand panel) in agreement with the slip distribution of Fig. 2. This main event triggered the offshore events (black arrow on the left-hand side). The Mejillones offshore seismicity (plotted in blue) remained active longer than the main rupture plotted in red. Activity decreased after the first 2 weeks to restart 3 d before the Michilla earthquake with a 6.1 thrust event that preceded the Michilla event (black arrow to the right-hand side). Events of $M_L > 6$ are shown with yellow stars.

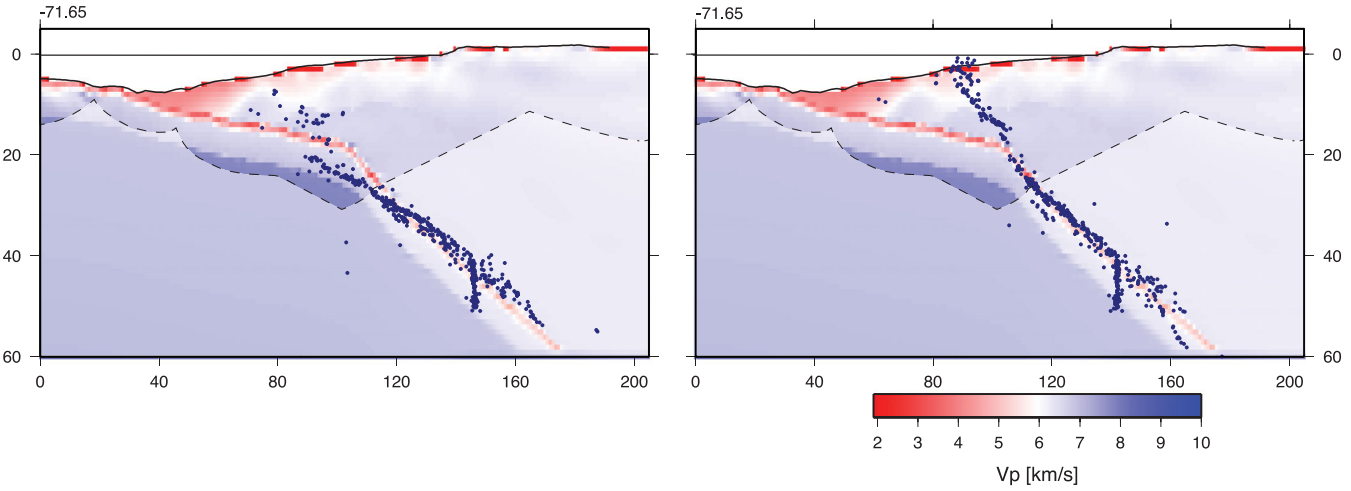

Figure 9. The aftershock distribution of the 2007 Tocopilla earthquake superimposed on the velocity model recently proposed by Contreras-Reyes *et al.* (2012) for the latitude 22°S. Our locations are centred on the Mejillones peninsula. On the left-hand side, we plot the aftershock locations obtained with a 1-D layered velocity model proposed by Husen *et al.* (1999). On the right-hand side, locations determined using the 2-D model proposed by Patzwahl *et al.* (1999). The velocity model proposed by Contreras-Reyes *et al.* (2012) is well defined above the the dashed-line. The two aftershock distributions are very similar at depth, delineating the same planar zone situated near the top of the oceanic crust of the subducted Nazca Plate. At shallower depths, the locations differ significantly but we consider that these aftershocks were not well located because of the lack of ocean bottom instruments.

Schurr *et al.* (2012) found some normal fault mechanisms in the upper plate from waveform modelling, but we could not confirm their results because fault plane solution were not well constrained in the southern part of the aftershock sequence during the two first weeks. Although we looked carefully for shallow aftershocks in our data we could not find a single well located event in the region close to the coast. This is in stark contrast with the seismicity produced by the Maule M_w 8.8 earthquake of 2010 February 27 whose

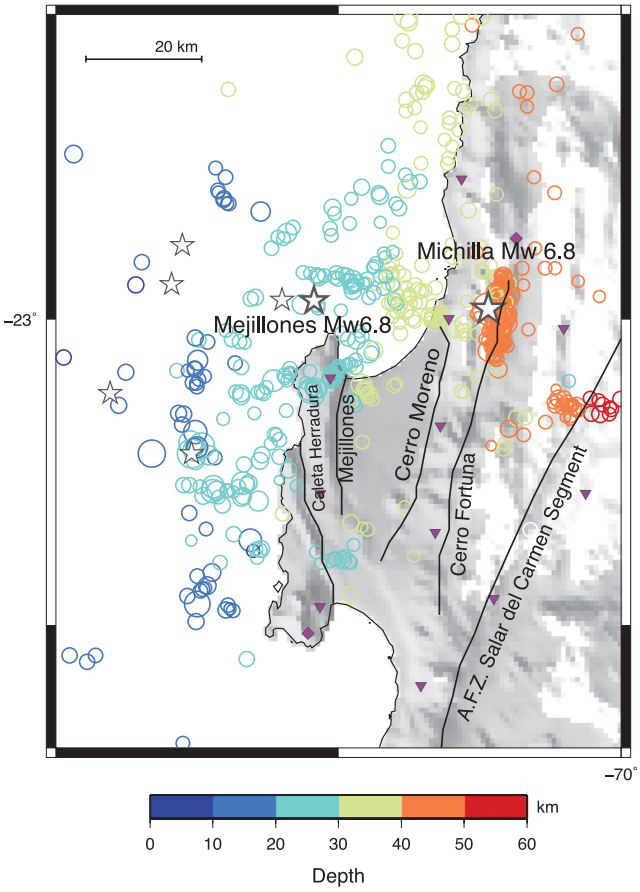

Figure 10. 1-D Locations in the Mejillones peninsula zone. This peninsula has well-known geological structures plotted on the map (Armijo & Thiele 1990). We did not find any shallow aftershocks associated with these structures.

largest aftershock was an event that occurred on a shallow fault near Pichilemu (Farías *et al.* 2011). Although the aftershocks or the Maule earthquake have not been fully relocated yet, the studies by Lange *et al.* (2012) and Rietbrock *et al.* (2012) have reported many shallow and quite a few deep aftershocks. The rupture zone delineated by the aftershock distribution seems to be much wider in Maule than in Tocopilla. Part of the difference may simple be that a very large event like Maule necessarily breaks a broad zone of the plate interface and produces many aftershocks away from this seismogenic zone. In Tocopilla, we observe that the aftershocks occurred in a very thin zone at the contact between the Nazca and South American plates. It is possible that the localization of aftershocks in a narrow zone is very different for megathrust events and regular subduction events like Tocopilla.

The Michilla slab-push earthquake and its aftershocks occurred near the centre of the network so that their focal mechanisms are very well determined. The rupture zone of this event was an almost vertical, planar zone very well defined by the aftershocks. These slab-compression events have been observed several times in Chile (Astiz & Kanamori 1986; Lemoine et al. 2002; Gardi *et al.* 2006), but this is the first time that the rupture plane is so well delineated by the distribution of the aftershocks. The majority of these aftershocks had very similar mechanisms as those of the main event. They ruptured a compact zone of 14 km length by 11 km depth with the hypocentre situated in the centre. This rupture zone extends from the top of the megathrust seismogenic zone to a depth that is probably very close to the base of the oceanic crust. In Fig. 5, we compare our locations with the results of a receiver functions sections obtained by Sodoudi *et al.* (2011). This slab push earthquake occurred below the second patch of the mainshock and was very likely triggered by stress transfer from the main shock as discussed by Peyrat *et al.* (2010). It occurred 3 d after a reactivation of the aftershock seismicity offshore the Mejillones peninsula as observed in Fig. 8. This reactivation occurred when the aftershocks of the Tocopilla main event had significantly diminished. The Michilla earthquake had its own set of aftershocks and foreshocks that remained very close to the rupture zone of the earthquake at least during the 2 d that we studied. Of all slab-push events in Chile, the Punitaqui earthquake of 1997 October 15 (Lemoine *et al.* 2002; Gardi *et al.* 2006) is the most similar to Michilla, at least in size and position with respect to the transition zone in Chile. As for Michilla, the Punitaqui earthquake was preceded by a series of thrust events near the centre of the seismogenic zone on the plate interface. Those events, however, occurred as a swarm in 1997 July at a distance of more than 50 km from the Punitaqui hypocentre. For both events we claim that stress reduction on the plate interface loaded the region near the tip of the transition zone, where slip occurs continuously, triggering these slab push earthquakes inside the subducted Nazca Plate.

8 CONCLUSIONS

We studied the aftershock distribution of the 2007, M_w 7.7 Tocopilla earthquake of Northern Chile. We used data from a sparse permanent network of stations (IPOC) and a dense temporary array (TF) to locate the aftershocks, determine their magnitude and identify their mechanisms. The aftershocks define an activated zone of about 160 km of length in north-south direction by 25 km of width in the northern area near the down-dip limit of the seismogenic zone, and a broad zone in the southern part of the rupture of about 50 km of large. Using *P* and *S* phases individually read from seismograms and a double-difference method, we could significantly improve the locations. We found that the aftershocks of the Tocopilla earthquake are distributed on a very narrow seismogenic zone at the interface between the Nazca and South American plates. The vertical cross-section of the seismicity depends significantly on the velocity model used for the locations. The simpler 1-D model produces a curved interface that smoothly reaches the trench, while a 2-D velocity model derived from a local seismic experiment produces a seismogenic interface that intersects the surface far from the trench. We can not resolve the differences between these two velocity models because the off-shore locations are less accurate than the inland ones. To improve the quality of the offshore locations and better image the geometry of the slab we would have required ocean bottom instruments. Our study confirms the previous work by Peyrat *et al.* (2010); Béjar-Pizarro *et al.* (2010) who proposed that the Tocopilla earthquake broke the bottom of the plate interface, just above the transition zone. The plate interface in the Tocopilla region did not have a large earthquake in at least 135 yr since the great Iquique earthquake of 1977. A possible scenario is that the rupture of the bottom part of the seismogenic zone may have increased the risk of a future tsunamigenic earthquake that will break the entire plate interface. We cannot exclude however an alternative scenario in which a series of earthquakes of magnitude close to 8 may occur along the coast of the northern Chile gap delaying the occurrence of a very large megathrust earthquake. Future observations will permit us to decide which of these two scenarios is more likely in Northern Chile.

ACKNOWLEDGEMENTS

This research was carried out under the Montessus de Ballore International Laboratory established between the University of Chile and the Centre National de la Recherche Scientifique (CNRS) in France. This work was supported by FONDECYT No. 1100429 in Chile and by ANR project S4 in France. AF was supported by a fellowship from AXA. We thank the many researchers in Chile, Germany and France that have installed and maintained seismic networks in Northern Chile, in particular GFZ that makes the IPOC data openly available from the GEOFON website.We deeply thank Sergio Ruiz and Claudio Satriano for numerous discussions. The manuscript was improved thanks to the constructive comments of the editor and two anonymous referees. We used the Generic Mapping Tool (http://gmt.soest.hawaii.edu/) to prepare many of the figures.

REFERENCES

Allen, R., 1978. Automatic earthquake recognition and timing from single traces, *Bull. seism. Soc. Am.,* **68**(5), 1521–1532.

Angermann, D., Klotz, J. & Reigber, C., 1999. Space-geodetic estimation of the Nazca-south America Euler vector, *Earth planet. Sci. Lett.,* **171**(3), 329–334.

Armijo, R. & Thiele, R., 1990. Active faulting in northern Chile: ramp stacking and lateral decoupling along a subduction plate boundary?, *Earth planet. Sci. Lett.,* **98**(1), 40–61.

Astiz, L. & Kanamori, H., 1986. Interplate coupling and temporal variation of mechanisms of intermediate-depth earthquakes in Chile, *Bull. seism. Soc. Am.,* **76**(6), 1614–1622.

Baer, M. & Kradolfer, U., 1987. An automatic phase picker for local and teleseismic events, *Bull. seism. Soc. Am,* **77**(4), 1437–1445.

Béjar-Pizarro, M. *et al.*, 2010. Asperities and barriers on the seismogenic zone in North Chile: state-of-the-art after the 2007 Mw 7.7 Tocopilla earthquake inferred by GPS and InSAR data, *Geophys. J. Int.,* **183**(1), 390–406.

Bobbio, A., Vassallo, M. & Festa, G., 2009. A local magnitude scale for southern Italy, *Bull. seism. Soc. Am.,* **99**(4), 2461–2470.

Brune, J., 1970. Tectonic stress and the spectra of seismic shear waves from earthquakes, *J. geophys. Res.,* **75**(26), 4997–5009.

Chlieh, M., De Chabalier, J., Ruegg, J., Armijo, R., Dmowska, R., Campos, J. & Feigl, K., 2004. Crustal deformation and fault slip during the seismic cycle in the North Chile subduction zone, from GPS and InSAR observations, *Geophys. J. Int.,* **158**(2), 695–711.

Chlieh, M. *et al.*, 2011. Interseismic coupling and seismic potential along the Central Andes subduction zone, *J. geophys. Res.,* **116**(B12), B12405, doi:10.1029/2010JB008166.

Cifuentes, I., 1989. The 1960 Chilean earthquakes, *J. geophys. Res.,* **94**(B1), 665–680.

Comte, D. & Pardo, M., 1991. Reappraisal of great historical earthquakes in the northern Chile and southern Peru seismic gaps, *Nat. Hazards,* **4**(1), 23–44.

Comte, D., Eisenberg, A., Lorca, E., Pardo, M., Ponce, L., Saragoni, R., Singh, S. & Suárez, G., 1986. The 1985 central Chile earthquake: a repeat of previous great earthquakes in the region?, *Science,* **233**(4762), 449–453.

Comte, D., Pardo, M., Dorbath, L., Dorbath, C., Haessler, H., Rivera, L., Cisternas, A. & Ponce, L., 1994. Determination of seismogenic interplate contact zone and crustal seismicity around Antofagasta, northern Chile using local data, *Geophys. J. Int.,* **116**(3), 553–561.

Contreras-Reyes, E., Jara, J., Grevemeyer, I., Ruiz, S. & Carrizo, D., 2012. Abrupt change in the dip of the subducting plate beneath north Chile, *Nat. Geosci.,* **5**(5), 342–345.

Delouis, B., Cisternas, A., Dorbath, L., Rivera, L. & Kausel, E., 1996. The Andean subduction zone between 22 and 25 S (northern Chile): precise geometry and state of stress, *Tectonophysics,* **259**(1–3), 81–100.

Delouis, B. *et al.*, 1997. The Mw = 8.0 Antofagasta (northern Chile) earthquake of 30 July 1995: a precursor to the end of the large 1877 gap, *Bull. seism. Soc. Am.,* **87**(2), 427–445.

Delouis, B., Pardo, M., Legrand, D. & Monfret, T., 2009. The Mw 7.7 Tocopilla earthquake of 14 November 2007 at the southern edge of the northern Chile seismic gap: rupture in the deep part of the coupled plate interface, *Bull. seism. Soc. Am.,* **99**(1), 87–89.

Dorbath, L., Cisternas, A. & Dorbath, C., 1990. Assessment of the size of large and great historical earthquakes in Peru, *Bull. seism. Soc. Am.,* **80**(3), 551–576.

Farías, M., Comte, D., Roecker, S., Carrizo, D. & Pardo, M., 2011. Crustal extensional faulting triggered by the 2010 Chilean earthquake: the Pichilemu seismic sequence, *Tectonics,* **30**(6), doi:10.1029/2011TC002888.

Gardi, A., Lemoine, A., Madariaga, R. & Campos, J., 2006. Modeling of stress transfer in the Coquimbo region of central Chile, *J. geophys. Res.,* **111,** B04307, doi:10.1029/2004JB003440.

Giovanni, M., Beck, S. & Wagner, L., 2002. The June 23, 2001 Peru earthquake and the southern Peru subduction zone, *Geophys. Res. Lett.,* **29**(21), 14–1.

Goldstein, P., Dodge, D., Firpo, M. & Minner, L., 2003. SAC2000: signal processing and analysis tools for seismologists and engineers, *Int. Geophys.,* **81,** 1613–1614.

Husen, S., Kissling, E., Flueh, E. & Asch, G., 1999. Accurate hypocentre determination in the seismogenic zone of the subducting Nazca Plate in northern Chile using a combined on-/offshore network, *Geophys. J. Int.,* **138**(3), 687–701.

Husen, S., Kissling, E. & Flueh, E., 2000. Local earthquake tomography of shallow subduction in north Chile—a combined onshore and offshore study, *J. geophys. Res.,* **105**(B12), 28 183–28 198.

Kanamori, H. & Cipar, J., 1974. Focal process of the great Chilean earthquake May 22, 1960, *Phys. Earth planet. Inter.,* **9**(2), 128–136.

Kanamori, H. & Jennings, P., 1978. Determination of local magnitude, ML, from strong-motion accelerograms, *Bull. seism. Soc. Am.,* **68**(2), 471–485.

Kausel, E., 1986. Los terremotos de agosto de 1868 y mayo de 1877 que afectaron el sur del perú y norte de chile, *Boletín de la Academia Chilena de Ciencias,* **3,** 8–14.

Kelleher, J., Sykes, L. & Oliver, J., 1973. Possible criteria for predicting earthquake locations and their application to major plate boundaries of the pacific and the caribbean, *J. geophys. Res.,* **78**(14), 2547–2585.

Klotz, J. *et al.*, 1999. GPS-derived deformation of the Central Andes including the 1995 Antofagasta Mw = 8.0 earthquake, *Pure appl. Geophys.,* **154**(3–4), 709–730.

Lancieri, M., Fuenzalida, A., Ruiz, S. & Madariaga, R., 2011. Magnitude scaling of early-warning parameters for the Mw 7.8 Tocopilla, Chile, earthquake and its aftershocks, *Bull. seism. Soc. Am.,* **101**(2), 447–463.

Lancieri, M., Madariaga, R. & Bonilla, F., 2012. Spectral scaling of the aftershocks of the Tocopilla 2007 earthquake in northern Chile, *Geophy. J. Int.,* **189**(1), 469–480.

Lange, D. *et al.*, 2012. Aftershock seismicity of the 27 February 2010 Mw 8.8 Maule earthquake rupture zone, *Earth planet. Sci. Let.,* **317**(318), 413–425.

Lemoine, A., Madariaga, R. & Campos, J., 2002. Slab-pull and slab-push earthquakes in the Mexican, Chilean and Peruvian subduction zones, *Phys. Earth planet. Int.,* **132**(1), 157–175.

Lomax, A., Virieux, J., Volant, P. & Berge, C., 2000. Probabilistic earthquake location in 3D and layered models: introduction of a Metropolis-Gibbs method and comparison with linear locations, in *Advances in Seismic Event Location,* pp. 101–134, eds, Thurber, C.H. & Rabinowitz, N., Kluwer, Amsterdam.

Lomax, A., Satriano, C. & Vassallo, M., 2012. Automatic picker developments and optimization: filterpickera robust, broadband picker for real-time seismic monitoring and earthquake early warning, *Seism. Res. Lett.,* **83**(3), 531–540.

Lomnitz, C., 1971. Grandes terremotos y tsunamis en Chile durante el periodo 1535-1955, *Geofis. Panamericana,* **1,** 151–171.

Madariaga, R., Métois, M., Vigny, C. & Campos, J., 2010. Central Chile finally breaks, *Science,* **328**(5975), 181–182.

Malgrange, M. & Madariaga, R., 1983. Complex distribution of large thrust and normal fault earthquakes in the Chilean subduction zone, *Geophys. J. R. astr. Soc.,* **73**(2), 489–505.

Montessus de Balore, F., 1911–1916. *Historia sismica de los Andes meridionales al sur del paralelo XVI,* Vol. 6, Cervantes, Santiago de Chile.

Motagh, M., Schurr, B., Anderssohn, J., Cailleau, B., Walter, T., Wang, R. & Villotte, J., 2010. Subduction earthquake deformation associated with 14 November 2007, Mw 7.8 Tocopilla earthquake in Chile: results from InSAR and aftershocks, *Tectonophysics,* **490**(1), 60–68.

Nippress, S. & Rietbrock, A., 2007. Seismogenic zone high permeability in the Central Andes inferred from relocations of micro-earthquakes, *Earth planet. Sci. Lett.,* **263**(3–4), 235–245.

Nishenko, S., 1985. Seismic potential for large and great interplate earthquakes along the Chilean and southern Peruvian margins of South America: a quantitative reappraisal, *J. geophys Res.,* **90**(B5), 3589–3615.

Patzwahl, R., Mechie, J., Schulze, A. & Giese, P., 1999. Two-dimensional velocity models of the Nazca plate subduction zone between 19.5 S and 25 S from wide-angle seismic measurements during the CINCA95 project, *J. geophys. Res.,* **104**(B4), 7293–7317.

Peyrat, S., Madariaga, R., Buforn, E., Campos, J., Asch, G. & Vilotte, J., 2010. Kinematic rupture process of the 2007 tocopilla earthquake and its main aftershocks from teleseismic and strong-motion data, *Geophys. J. Int.,* **182**(3), 1411–1430.

Pritchard, M., Simons, M., Rosen, P., Hensley, S. & Webb, F., 2002. Co-seismic slip from the 1995 July 30 Mw = 8.1 Antofagasta, Chile, earthquake as constrained by InSAR and GPS observations, *Geophys. J. Int.,* **150**(2), 362–376.

Reasenberg, P. & Oppenheimer, D., 1985. FPFIT, FPPLOT, and FPPAGE: fortran computer programs for calculating and displaying earthquake fault-plane solutions, US Dept. of the Interior, Geological Survey.

Richter, C., 1935. An instrumental earthquake magnitude scale, *Bull. seism. Soc. Am.,* **25**(1), 1–32.

Rietbrock, A., Ryder, I., Hayes, G., Haberland, C., Comte, D., Roecker, S. & Lyon-Caen, H., 2012. Aftershock seismicity of the 2010 Maule Mw = 8.8, Chile, earthquake: correlation between co-seismic slip models and aftershock distribution?, *Geophys. Res. Lett.,* **39**(8), doi:10.1029/2012GL051308.

Ruegg, J. *et al.*, 1996. The Mw = 8.1 Antofagasta (North Chile) earthquake of July 30, 1995: first results from teleseismic and geodetic data, *Geophys. Res. Lett,* **23**(9), 917–920.

Ruegg, J. *et al.*, 2009. Interseismic strain accumulation measured by GPS in the seismic gap between Constitución and Concepción in Chile, *Phys. Earth planet. Int.,* **175**(1–2), 78–85.

Ruiz, S. & Madariaga, R., 2011. Determination of the friction law parameters of the Mw 6.7 Michilla earthquake in northern Chile by dynamic inversion, *Geophys. Res. Lett.,* **38**(9), L09317, doi:10.1029/2011GL047147.

Schurr, B., Asch, G., Rosenau, M., Wang, R., Oncken, O., Barrientos, S., Salazar, P. & Vilotte, J., 2012. The 2007 M7. 7 Tocopilla northern Chile earthquake sequence: implications for along-strike and downdip rupture segmentation and megathrust frictional behavior, *J. geophys. Res.,* **117**(B5), B05305, doi:10.1029/2011JB009030.

Sobiesiak, M. *et al.*, 2008. The m 7.7 tocopilla earthquake and its aftershock sequence: deployment of a task force local network, *EOS Trans. AGU,* **89**(23), Jt. Assembly Suppl. Abstract S24A-04.

Sodoudi, F., Yuan, X., Asch, G. & Kind, R., 2011. High-resolution image of the geometry and thickness of the subducting Nazca lithosphere beneath northern Chile, *J. geophys. Res.,* **116,** B04302, doi:10.1029/2010JB007829.

Vargas, G., Palacios, C., Reich, M., Luo, S., Shen, C.-C., González, G. & Wu, Y.-C., 2011. U-series dating of co-seismic gypsum and submarine paleoseismology of active faults in northern Chile (23 s), *Tectonophysics,* **497**(1), 34–44.

Victor, P., Sobiesiak, M., Glodny, J., Nielsen, S. & Oncken, O., 2011. Long-term persistence of subduction earthquake segment boundaries: evidence from Mejillones Peninsula, northern Chile, *J. geophys. Res.,* **116**(B2), B02402, doi:10.1029/2010JB007771.

Vigny, C. *et al.*, 2011. The 2010 Mw 8.8 maule megathrust earthquake of Central Chile, Monitored by GPS, *Science,* **332**(6036), 1417–1421.

Waldhauser, F. & Ellsworth, W., 2000. A double-difference earthquake location algorithm: method and application to the northern Hayward fault, California, *Bull. seism. Soc. Am.,* **90**(6), 1353–1368.

SUPPORTING INFORMATION

Additional Supporting Information may be found in the online version of this article:

Figure S1. *P*-wave velocity model used for the location of the 2007 Tocopilla aftershocks.
Figure S2. Error distibution of aftershock locations of the 2007 Tocopilla earthquake.
Figure S3. Aftershocks of the 2007 Tocopilla earthquake.
Figure S4. Determination of the Gutenberg–Richter law for the Tocopilla aftershocks.
Figure S5. Zoom on the aftershock zone of the 2007 December 16 Michilla earthquake (http://gji.oxfordjournals.org/lookup/suppl/doi:10.1093/gji/ggt163/-/DC1).

Please note: Oxford University Press is not responsible for the content or functionality of any supporting materials supplied by the authors. Any queries (other than missing material) should be directed to the corresponding author for the article.